Supplementary Material: Collective ballistic motion explains fast aggregation in adhesive active matter

Emanuel F. Teixeira,* Carine P. Beatrici,† Heitor C. M. Fernandes,‡ and Leonardo G. Brunnet§
Instituto de Física, Universidade Federal do Rio Grande do Sul, CP 15051, CEP 91501-970 Porto Alegre - RS, Brazil

P. de Castro¶
ICTP South American Institute for Fundamental Research, Instituto de Física Teórica, UNESP – Universidade Estadual Paulista, Rua Dr. Bento T. Ferraz 271, 01140-070, São Paulo, SP, Brazil

ADDITIONAL SIMULATION DETAILS

We use $k_c = 200v_0/(\sigma\mu)$, $k_{\rm adh} = 10v_0/(\sigma\mu)$, $v_0 = 0.1$, $\mu = 1$, $\sigma = 1$ and $l_{\rm adh} = 1.5\sigma$. Thus, particles irreversibly bind when they meet: the lowest adhesion, $k_{\rm adh}\sigma$, is 10 times the self-propulsion, v_0/μ, so particles move only in directions that do not destroy binding. We employ the Euler-Maruyama algorithm with a time step $\Delta t = 0.001\tau_0$.

CLUSTER MASS DISTRIBUTIONS AND DYNAMICAL SCALING

We present here our results for the effect of the alignment strength J on the cluster mass distribution $P(M,t)$ in the low (Pe = 1) and high Péclet number regimes (Pe = 10^3).

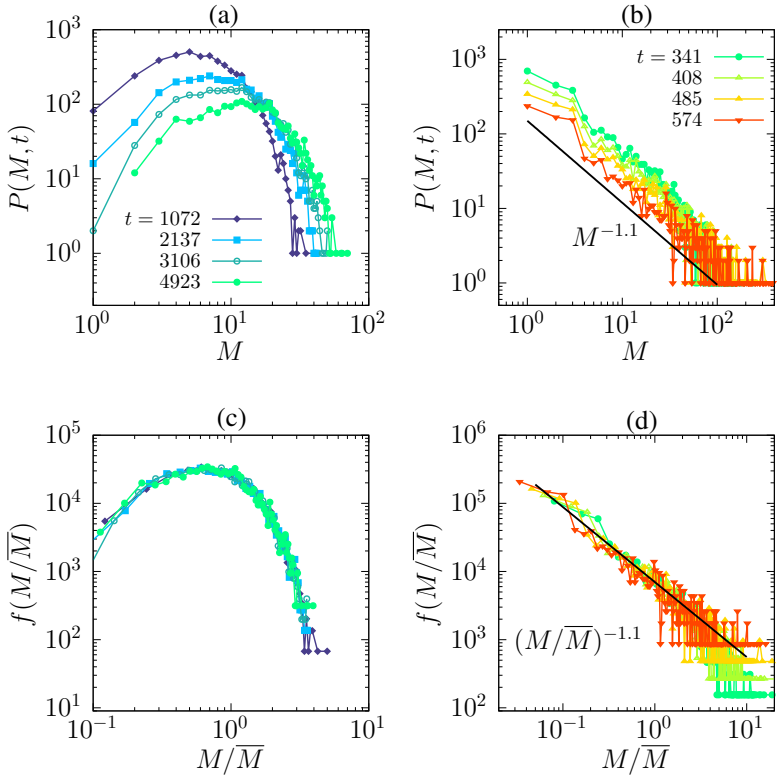

FIG. S1. Cluster mass distribution $P(M,t)$ in the high Péclet number regime (Pe = 10^3). (a) For $J = 0$, below the flocking threshold, the distribution has a peak, reflecting a characteristic cluster size. (b) For $J = 100$, above the flocking transition, the distribution becomes power-law, $P(M,t) \sim M^{-\lambda}$, with $\lambda \simeq 1.1$. For (c) $J = 0$ and (d) $J = 100$, the rescaled distributions collapse onto a single curve, $f(M/\overline{M}) = \overline{M}^2 P(M,t)$, confirming dynamical scaling [1].

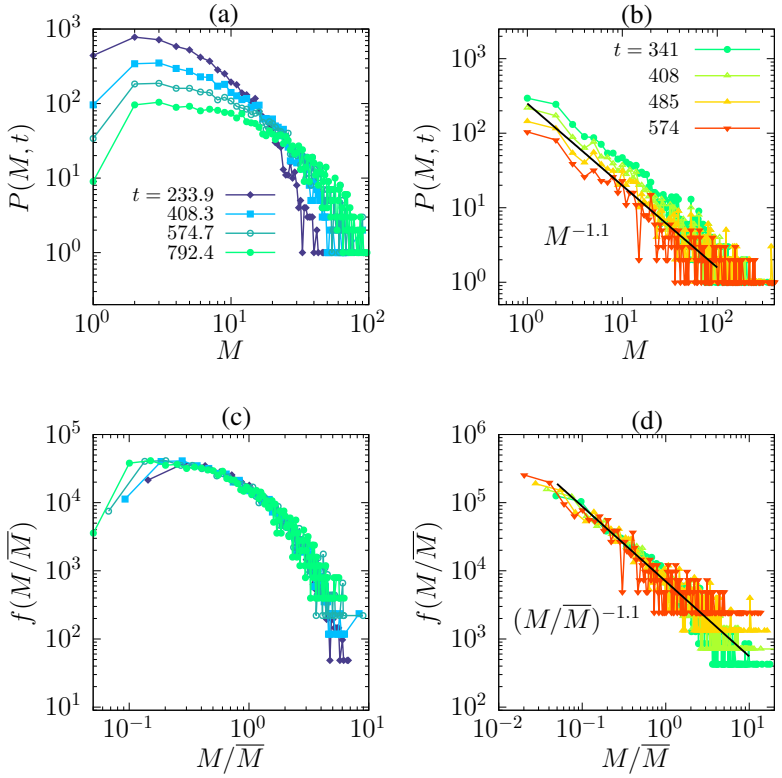

FIG. S2. Similar to Figure S1, now in the high Péclet number regime (Pe = 10^3).

Figures S1a and b show $P(M,t)$ for different time instants after the system has entered the algebraic coarsening regime [1], for low Pe. For $J = 0$, below the flocking transition, the distribution exhibits a non-monotonic shape, indicating the presence of a characteristic cluster size. In contrast, for strong alignment ($J = 100$), the distribution develops a power-law tail, $P(M,t) \sim M^{-\lambda}$, with exponent $\lambda \simeq 1.1$, consistent with scale-free cluster growth driven by collective motion. We observe in Figures S1c and d that the distributions obey dynamical scaling. When rescaled by the mean cluster mass $\overline{M}(t)$, all curves collapse onto a single universal function, $f\left(\frac{M}{\overline{M}}\right) = \overline{M}^2 P(M,t)$, demonstrating self-similar evolution during the coarsening process. The same universal scaling function was observed in Ref. [1] for another irreversible aggregation problem. For high Pe, the behavior of the cluster mass distributions is similar; see Figure S2.

CLUSTER AGGREGATION THEORY: THE SMOLUCHOWSKI COAGULATION EQUATION

We present here a cluster aggregation theory based on the Smoluchowski coagulation equation [2] generalized to the types of mass-dependent cluster movements of our problem. This theoretical approach builds on the derivation presented in Ref. [1], incorporating modifications where appropriate. For completeness, we include intermediate steps common to other irreversible aggregation problems. Consider clusters with different masses moving through space. When two clusters of masses M and M' come sufficiently close, they may irreversibly merge into a single cluster of mass $M + M'$:

$$A_M + A_{M'} \xrightarrow[K(M,M')]{} A_{M+M'}. \tag{1}$$

Here, A_M denotes a cluster and $K(M,M')$ denotes the rate at which two clusters of masses M and M' coagulate. This quantity is known as the coagulation kernel.

We assume a continuous mean-field approach characterized by spatial homogeneity, where the cluster mass distribution is uniform throughout the entire space:

$$\int_{V_0} P(\mathbf{r}, M, t)\, dV = P(M,t) V_0, \tag{2}$$

where $P(M,t)$ is the spatially-homogeneous cluster mass distribution and $V_0 = L^d$ is the total d-dimensional hypercubic volume. Notice that, while our simulations were performed in $d = 2$, consistent with many experimental setups, we formulate the theory in arbitrary dimension d, as the generalization is straightforward. We now define the concentration of the mass distribution as

$$C(M,t) = \frac{P(M,t)}{V_0}. \tag{3}$$

The concentration $C(M,t)$ increases when two smaller clusters of masses M' and $M - M'$ merge to form a cluster of mass M. The rate of this process is proportional to the product $C(M',t)\, C(M-M',t)$. On the other hand, when a cluster of mass M merges with any other cluster, it is removed from the population, resulting in a decrease in $C(M,t)$. To describe the full aggregation process, we integrate over the coagulating masses, treated as continuous variables:

$$\frac{\partial C(M,t)}{\partial t} = \frac{1}{2}\int_0^M K(M', M-M')\, C(M',t)\, C(M-M',t)\, dM' - \int_0^\infty K(M,M')\, C(M,t)\, C(M',t)\, dM', \tag{4}$$

where $K(M,M')$ is the coagulation kernel. The prefactor $1/2$ ensures that the contribution is not double-counted. Equation (4) is the Smoluchowski coagulation equation [2]. In terms of the mass distribution $P(M,t)$, Eq. (4) becomes

$$\frac{\partial P(M,t)}{\partial t} = \frac{1}{2\,V_0}\int_0^M K(M', M-M')\, P(M',t)\, P(M-M',t)\, dM' - \frac{1}{V_0}\int_0^\infty K(M,M')\, P(M,t)\, P(M',t)\, dM'. \tag{5}$$

We note that the total mass is conserved:

$$M_0 = \int_0^\infty M\, P(M,t)\, dM = \text{const}. \tag{6}$$

Also, we define the total number of clusters:

$$N(t) = \int_0^\infty P(M,t)\, dM. \tag{7}$$

Using Eq. (5), we compute the time derivative of $N(t)$:

$$\begin{aligned}\frac{dN(t)}{dt} = {} & \frac{1}{2\,V_0}\int_0^\infty \int_0^M K(M', M-M')\, P(M',t)\, P(M-M',t)\, dM'\, dM \\ & -\frac{1}{V_0}\int_0^\infty \int_0^\infty K(M,M')\, P(M,t)\, P(M',t)\, dM'\, dM.\end{aligned} \tag{8}$$

We now interchange the order of integration in the first term and perform the change of variables $M'' = M - M'$:

$$\begin{aligned}\frac{dN(t)}{dt} = {} & \frac{1}{2\,V_0}\int_0^\infty \int_0^\infty K(M', M'') P(M',t) P(M'',t)\, dM''\, dM' \\ & -\frac{1}{V_0}\int_0^\infty \int_0^\infty K(M,M') P(M,t) P(M',t)\, dM'\, dM.\end{aligned} \tag{9}$$

Renaming dummy variables $M' \to M$ and $M'' \to M'$, this becomes

$$\frac{dN(t)}{dt} = -\frac{1}{2\,V_0}\int_0^\infty \int_0^\infty K(M,M') P(M,t) P(M',t)\, dM'\, dM. \tag{10}$$

The average cluster mass is defined as

$$\overline{M}(t) = \frac{\int_0^\infty M P(M,t)\, dM}{\int_0^\infty P(M,t)\, dM} = \frac{M_0}{N(t)}. \tag{11}$$

Thus,

$$N(t) = \frac{M_0}{\overline{M}(t)}. \tag{12}$$

Taking the time derivative yields

$$\frac{dN(t)}{dt} = -\frac{M_0}{\overline{M}(t)^2}\frac{d\overline{M}(t)}{dt}. \tag{13}$$

Substituting Eq. (13) into Eq. (10) leads to

$$\frac{d\overline{M}(t)}{dt} = \frac{\overline{M}(t)^2}{2\,M_0\,V_0}\int_0^\infty\int_0^\infty K(M,M')P(M,t)P(M',t)\,dM'\,dM. \tag{14}$$

Diffusion-limited cluster aggregation

The physical processes governing the rate of cluster coagulation vary depending on the specific scenario. We first focus on diffusion-limited aggregation, where cluster diffusion governs the coagulation rate. Other factors such as cluster shape and collision cross-section can also be incorporated. For a sphere of radius R surrounded by Brownian particles with diffusion constant D, the absorption rate scales as $K \sim DR^{d-2}$ [3]. Based on this idea, a widely used kernel for DLCA [1, 4–6] is

$$K(M,M') = A\left[D(M)+D(M')\right]\left[R(M)+R(M')\right]^{d-2} = A\left(M^\alpha + M'^\alpha\right)\left(M^{1/d_f}+M'^{1/d_f}\right)^{d-2}, \tag{15}$$

where A is a constant that ensures correct dimensionality (volume/time), $R \sim M^{1/d_f}$ is the radius of gyration with fractal dimension d_f, and $D(M) \sim M^\alpha$ is the diffusion-mass scaling (observed in our simulations here and in other references such as Ref. [7]). Unlike fixed spheres absorbing particles, here clusters themselves diffuse and merge, thus the kernel includes sums of diffusion constants and radii.

Substituting Eq. (15) into Eq. (14), we get

$$\frac{d\overline{M}(t)}{dt} = \frac{A\,\overline{M}(t)^2}{2\,M_0\,V_0}\int_0^\infty\int_0^\infty \left(M^\alpha + M'^\alpha\right)\left(M^{1/d_f}+M'^{1/d_f}\right)^{d-2}P(M,t)P(M',t)\,dM'\,dM. \tag{16}$$

From our simulations, as discussed above, we observe the dynamical scaling form [1]

$$P(M,t) = \overline{M}(t)^{-2} f\left(\frac{M}{\overline{M}(t)}\right). \tag{17}$$

Applying the change of variables $x = M/\overline{M}(t)$ and $x' = M'/\overline{M}(t)$, Eq. (16) becomes

$$\begin{aligned}\frac{d\overline{M}(t)}{dt} &= \frac{A\overline{M}(t)^{\alpha+\frac{d-2}{d_f}}}{2M_0V_0}\int_0^\infty\int_0^\infty (x^\alpha + x'^\alpha)(x^{1/d_f}+x'^{1/d_f})^{d-2}f(x)f(x')\,dx\,dx' \\ &= C_1\overline{M}(t)^{\alpha+\frac{d-2}{d_f}},\end{aligned} \tag{18}$$

where

$$I_1 = \int_0^\infty\int_0^\infty (x^\alpha + x'^\alpha)(x^{1/d_f}+x'^{1/d_f})^{d-2}f(x)f(x')\,dx\,dx' \tag{19}$$

is a constant, and

$$C_1 = \frac{AI_1}{2M_0V_0}. \tag{20}$$

Integrating Eq. (18) with initial condition $\overline{M}(0) = 1$ yields

$$\overline{M}(t) = \left[C_1\left(1-\alpha-\frac{d-2}{d_f}\right)t+1\right]^{\frac{d_f}{d_f-d_f\alpha-(d-2)}} \sim t^z, \tag{21}$$

with the dynamic exponent

$$z = \frac{d_f}{d_f - d_f\alpha - (d-2)}. \tag{22}$$

In two dimensions ($d = 2$), this simplifies to

$$z = \frac{1}{1-\alpha}. \tag{23}$$

Hence, the average cluster mass grows algebraically in time as a direct consequence of the dynamical scaling hypothesis.

Ballistic aggregation

In ballistic aggregation, cluster collisions are dominated by their relative velocity. A commonly used kernel in the literature is [1, 8]

$$K(M, M') = B\,|V(M) - V(M')|\,(R(M) + R(M'))^{d-1} = B\,|M^\gamma - M'^\gamma|\left(M^{1/d_f} + M'^{1/d_f}\right)^{d-1}. \tag{24}$$

Here, $|V(M) - V(M')|$ originates from the relative velocity between clusters and the term $(R(M) + R(M'))^{d-1}$ corresponds to their collision cross-section. As we observed in our simulations, the typical cluster speed scales with mass as $V \sim M^\gamma$. For clusters composed of particles with uncorrelated self-propulsions, $\gamma = -1/2$, whereas for fully aligned clusters, $\gamma = 0$.

Substituting Eq. (24) into Eq. (14) yields

$$\frac{d\overline{M}(t)}{dt} = \frac{B\overline{M}(t)^2}{2M_0V_0}\int_0^\infty\int_0^\infty |M^\gamma - M'^\gamma|\left(M^{1/d_f} + M'^{1/d_f}\right)^{d-1} P(M,t)P(M',t)\,dM'\,dM. \tag{25}$$

Applying the scaling ansatz Eq. (17), and changing variables as before, leads to

$$\begin{aligned}\frac{d\overline{M}(t)}{dt} &= \frac{B\overline{M}(t)^{\gamma+\frac{d-1}{d_f}}}{2M_0V_0}\int_0^\infty\int_0^\infty |x^\gamma - x'^\gamma|(x^{1/d_f} + x'^{1/d_f})^{d-1} f(x)f(x')\,dx\,dx' \\ &= C_2\overline{M}(t)^{\gamma+\frac{d-1}{d_f}},\end{aligned} \tag{26}$$

where

$$I_2 = \int_0^\infty\int_0^\infty |x^\gamma - x'^\gamma|(x^{1/d_f} + x'^{1/d_f})^{d-1} f(x)f(x')\,dx\,dx' \tag{27}$$

is a constant and

$$C_2 = \frac{BI_2}{2M_0V_0}. \tag{28}$$

Integrating Eq. (26) with $\overline{M}(0) = 1$ gives

$$\overline{M}(t) = \left[C_2\left(1 - \gamma - \frac{d-1}{d_f}\right)t + 1\right]^{\frac{d_f}{d_f - d_f\gamma - (d-1)}} \sim t^z, \tag{29}$$

where the dynamic exponent is

$$z = \frac{d_f}{d_f - d_f\gamma - (d-1)}. \tag{30}$$

Assuming compact, non-fractal clusters where the spatial dimension equals the fractal dimension, $d = d_f$, the dynamic exponent reduces to

$$z = \frac{d}{1 - d\gamma}. \tag{31}$$

Again, the average cluster mass grows algebraically in time with the exponent z depending on the scaling of speed, fractal dimension, and system dimension. For $d = 2$, we obtain $z = \frac{2}{1-2\gamma}$ as discussed in the main text. In particular, for non-collective ballistic aggregation, one has $\gamma = -1/2$ and we obtain $z = 1$.

MOVIES

For illustration, **Movie 1** shows the aggregation for (a) $J = 100$ and $\mathrm{Pe} = 1$, (b) $J = 100$ and $\mathrm{Pe} = 1000$, (c) $J = 0$ and $\mathrm{Pe} = 1$, and (d) $J = 0$ and $\mathrm{Pe} = 1000$. To facilitate visualization, we used $\phi = 0.1$. Colors indicate the polarization of the particles; for a color wheel, see main text. **Movie 2** shows single-cluster simulations for the same values of J and Pe.

The films reveal that cluster fractality becomes more pronounced at higher densities and extraordinary values of J. To observe fractality in the exponents z measured in our main text figures, simulations at exceptional scales of mass and time would be required. To verify that these effects indeed emerge at large masses, we modified the averaging procedure for the average cluster mass in order to weight larger clusters more strongly, and observed a slight increase in z that is consistent with the theory above.

* emanuel.teixeira@ufrgs.br
† carine@if.ufrgs.br
‡ heitor.fernandes@ufrgs.br
§ leon@if.ufrgs.br
¶ pablo.castro@unesp.br

[1] F. Leyvraz, Physics Reports **383**, 95 (2003).
[2] M. v. Smoluchowski, Z. Physik. **17**, 585 (1916).
[3] P. L. Krapivsky, S. Redner, and E. Ben-Naim, *A kinetic view of statistical physics* (Cambridge University Press, 2010).
[4] A. Moncho-Jordá, F. Martínez-López, M. Quesada-Pérez, M. Cabrerizo-Vílchez, and R. Hidalgo-Álvarez, Surface and Colloid Science , 113 (2004).
[5] A. Moncho-Jordá, F. Martınez-López, and R. Hidalgo-Álvarez, Physica A: Statistical Mechanics and its Applications **282**, 50 (2000).
[6] A. Moncho-Jordá, G. Odriozola, F. Martınez-López, A. Schmitt, and R. Hidalgo-Álvarez, The European Physical Journal E **5**, 471 (2001).
[7] C. P. Beatrici, R. M. de Almeida, and L. G. Brunnet, Physical Review E **95**, 032402 (2017).
[8] Y. Jiang and F. Leyvraz, Journal of Physics A: Mathematical and General **26**, L179 (1993).